Geophysical Research Letters

RESEARCH LETTER
10.1029/2018GL077346

Mineral Dust Instantaneous Radiative Forcing in the Arctic

A. Kylling[1], C. D. Groot Zwaaftink[1], and A. Stohl[1]

[1] NILU-Norwegian Institute for Air Research, Kjeller, Norway

Key Points:
- Arctic top of the atmosphere mineral dust radiative forcing (RF) is dominated by dust from Asia and Africa
- Deposited dust accounts for half of the top of the atmosphere RF and nearly all of the bottom of the atmosphere RF
- Most of the dust deposited and thus most of the bottom of the atmosphere RF is contributed by high-latitude dust sources

Supporting Information:
- Supporting Information S1

Correspondence to:
A. Kylling,
arve.kylling@nilu.no

Citation:
Kylling A., Groot Zwaaftink, C. D., & Stohl, A. (2018). Mineral dust instantaneous radiative forcing in the Arctic. *Geophysical Research Letters*, *45*. https://doi.org/10.1029/2018GL077346

Received 31 JAN 2018
Accepted 7 APR 2018
Accepted article online 19 APR 2018

Abstract Mineral dust sources at high and low latitudes contribute to atmospheric dust loads and dust deposition in the Arctic. With dust load estimates from Groot Zwaaftink et al. (2016, https://doi.org/10.1002/2016JD025482), we quantify the mineral dust instantaneous radiative forcing (IRF) in the Arctic for the year 2012. The annual-mean top of the atmosphere IRF is 0.225 W/m^2, with the largest contributions from dust transported from Asia south of 60°N and Africa. High-latitude (>60°N) dust sources contribute about 39% to top of the atmosphere IRF and have a larger impact (1 to 2 orders of magnitude) on IRF per emitted kilogram of dust than low-latitude sources. Mineral dust deposited on snow accounts for nearly all of the bottom of the atmosphere IRF of 0.135 W/m^2. More than half of the bottom of the atmosphere IRF is caused by dust from high-latitude sources, indicating substantial regional climate impacts rarely accounted for in current climate models.

Plain Language Summary Mineral dust sources at high and low latitudes contribute to atmospheric dust loads and dust deposition in the Arctic. We quantify the annual-mean radiative forcing (RF) in the Arctic to be 0.225 W/m^2 at the top of the atmosphere. The largest contributions are from dust transported from Asia south of 60°N and Africa. High-latitude (>60°N) dust sources contribute about 39% to top of the atmosphere RF and have a larger (1 to 2 orders of magnitude) impact on RF per emitted kilogram of dust. Mineral dust deposited on snow accounts for nearly all of the bottom of the atmosphere RF of 0.135 W/m^2. More than half of the bottom of the atmosphere RF is caused by dust from high-latitude sources, indicating substantial regional climate impacts rarely accounted for in current climate models.

1. Introduction

The polar regions experience relatively large temperature changes due to feedback processes leading to Arctic amplification of global climate change (Serreze & Francis, 2006). It has been suggested that mineral dust contributes to Arctic amplification (Lambert et al., 2013, and references therein). Atmospheric and cryospheric impurities, such as mineral dust and black carbon (BC), affect the amount of radiation absorbed and scattered by the atmosphere and reduce the albedo of surfaces covered by snow or ice (Qian et al., 2015). Recent decreases in the albedo of the Greenland ice sheet have been partly ascribed to increasing amounts of impurities (e.g., Dumont et al., 2014), and Wittmann et al. (2017) found substantial influence of mineral dust on the surface energy balance of Vatnajökull ice cap, Iceland. The radiative impacts of mineral dust must thus be known in order to assess its role in the temperature changes recently observed in the Arctic (Bindoff et al., 2013).

Globally, the radiative forcing (RF) of mineral dust is estimated to be smaller than for BC, that is, −0.10 (−0.30 to +0.10) W/m^2 for dust and +0.60 (+0.24 to +1.02) W/m^2 for BC (Myhre et al., 2013, their tables 8.4 and 8.SM.7, and Figure 8.17). Here the numbers for BC include fossil-fuel, biofuel, and biomass burning sources, while BC and dust forcing via aerosol-cloud interactions and surface albedo effects are not included. BC emissions have a large anthropogenic component, and thus, their role in Arctic climate change has recently received a lot of attention (Quinn et al., 2015, and references therein). In the Arctic the RF peaks in the spring. Over snow-covered surfaces north of 60°N over Eurasia, Flanner et al. (2009, their Figure 7) estimated the March–May RF due to BC deposited in snow to about 1.5–3.5 W/m^2. The surface RF of snow-deposited dust was found to be between 0.5 and 1.5 W m^{-2}. Estimates of annual-mean RF for atmospheric BC in the Arctic range from 0.07 to 0.63 W/m^2 and between 0.03 and 0.28 W/m^2 for BC in snow and sea ice (Quinn et al., 2015). While the annual RF from BC in snow is small, the reduction in snow albedo in the spring time leads to snow cover removal, resulting in a comparatively larger climate effect (Flanner et al., 2007;

Hansen et al., 2007). Goldenson et al. (2012) assessed influences of deposition of BC and dust in snow on the Arctic climate based on model simulations and found similar impacts of dust and BC. The emission of mineral dust is largely a natural phenomenon, and this may explain why its forcing of the Arctic climate has been studied less. Dust emissions respond to changes in wind speed, soil moisture, and other parameters affected by climate change and are influenced by human-induced changes in land cover and surface properties. Thus, their influence on Arctic climate also varies, involving potentially important feedback processes (Lambert et al., 2013).

The major dust sources are the low-latitude deserts, but there are also dust sources at high latitudes (Bullard et al., 2016). As shown by Groot Zwaaftink et al. (2016) based on model simulations that include high-latitude dust sources, in the Arctic the atmospheric dust loads are dominated by dust transported from Asia and Africa, whereas dust deposition is dominated by local high-latitude sources. This is due to the different vertical distribution of dust from these sources, with dust from high-latitude sources residing in the lower troposphere and dust from remote sources arriving mainly in the upper troposphere. Also, the seasonality is different, with remote dust peaking in spring and high-latitude dust peaking in fall (Groot Zwaaftink et al., 2016). However, high-latitude dust sources seem to be not well represented in global models that are normally used to quantify RF and climate impacts. There appears to be no dust mobilization at high latitudes in these models, and simulated dust deposition patterns seem uninfluenced by these source regions (e.g., Albani et al., 2014; Mahowald et al., 2006).

The aim of this study is to quantify the instantaneous radiative forcing (IRF) in the Arctic of the dust from high-latitude sources and compare it with the IRF of dust from low-latitude sources using the dust load estimates (including high-latitude dust) from Groot Zwaaftink et al. (2016). The effects of dust in the atmosphere and deposited dust in snow are quantified together and separately.

2. Methods

Monthly dust concentrations were adopted from Groot Zwaaftink et al. (2016) whose simulations consisted of two steps: (1) Mineral dust emissions were calculated with the FLEXDUST emission module based on global land cover data and a friction-velocity-based formulation of dust emission (Marticorena & Bergametti, 1995; Shao & H. Lu, 2000) with size distribution from Kok (2011). The FLEXDUST dust emission was modified by soil moisture and snow cover and enhanced in topographical depressions. (2) Global transport and deposition of dust particles binned into 10 size classes were calculated using the Lagrangian particle dispersion model FLEXPART (Stohl et al., 2005). The simulations considered gravitational settling, dry and wet deposition, distinguishing between within-cloud and below-cloud scavenging as described in Grythe et al. (2017). The dust simulations were described in detail and evaluated against surface and airborne measurements by Groot Zwaaftink et al. (2016). At a few Arctic sites, monthly mean surface concentrations were shown to be estimated generally at the right order of magnitude. A comparison to aircraft observations indicated that concentrations are also represented realistically throughout the troposphere. Furthermore, dust deposition was compared to long-term records. For ice cores in Greenland, simulations tended to overestimate dust deposition. At three sites simulated, values of deposition in 2012 were within 1 order of magnitude from the long-term observations. At one site, with observed dust deposition amounts an order of magnitude smaller than at the other three sites, simulated deposition was a factor ~22 larger than the long-term average deposition. However, it should be considered that the ice core observations are in regions with rather little dust deposition and simulations do not cover the same period as observations. Additional FLEXPART simulations confirmed that Icelandic dust events are well represented (Groot Zwaaftink et al., 2017), but dust deposition on Vatnajökull ice cap in 1 year was overestimated by a factor 3 compared to observations (Wittmann et al., 2017). Overall, it seems that in the Arctic the FLEXPART simulations capture atmospheric concentrations quite well, but might overestimate dust deposition. However, the available measurement data are so limited and variable that a quantification of model bias is nearly impossible.

Liquid water and ice water clouds needed for the IRF calculations were taken from European Centre for Medium-Range Weather Forecast (ECMWF) operational analysis data. From the 6-hourly ECMWF fields monthly averaged cloud fields were constructed. See Text S1 in the supporting information and Key et al. (2002), Martin et al. (1994), McFarquhar et al. (2003), Yang et al. (2005), and Wyser, (1998) for further information.

For snow-free surfaces the surface albedo was taken from ECMWF analysis data, while for snow-covered land surfaces and sea ice, the albedo was calculated using the SNICAR model (Flanner et al., 2007, 2009) that allows incorporating the effects of snow impurities, including deposited dust and underlying surface albedo (see Text S2 and Varotsos et al., 2014; Wiscombe & Warren, 1980). Snow properties were taken from ECMWF except for snow grain size where we adopt a constant snow grain effective radius of 200 μm based on the maps of Aoki et al. (2007), Hori et al. (2007), and Stamnes et al. (2007) and sensitivity calculations (see Text S2). It is noted that this choice results in a high (low) bias in IRF of up to a factor of about 1.4 (0.7) for snow grain sizes smaller (larger) than about 100 μm (500 μm) for cloudless conditions in May at 75°N. For cloudy conditions the biases are reduced (see Figure S3, Text S2). Deposited dust was included in the SNICAR model by converting the FLEXDUST size bins to SNICAR size bins. Over land SNICAR was run in a two-layer configuration. If snow thickness increased from 1 month to another, the dust deposited that month was put in the top layer. Older dust was moved to the layer below. During snow melt dust was assumed to stay in the top layer. No removal of deposited dust was included. Over ocean dust on snow-covered sea ice was included as a single homogeneous snow layer (see Text S2 and Kern et al., 2015). It was assumed that all sea ice was snow covered. While the albedo of late season bare ice is certainly different from snow-covered ice, we justify this approach by noting that the dust IRF is largest in April – May when the sea ice is expected to be snow covered; and the dust IRF is smaller over ocean than over land. Dust optical properties were taken from the SNICAR model (dust optical properties are further discussed in Text S3, see also Balkanski et al., 2007 and Hess et al., 1998). Generally, dust lowers the albedo below wavelengths of about 1,000 nm. This is due to the wavelength dependence of the refractive index of dust. At 555 nm the real and imaginary parts of the refractive index were 1.51156 and 0.00187, respectively. The dust particles were assumed to be spherical (Nousiainen, 2009; Räisänen et al., 2013; Wang et al., 2013; Yi et al., 2011; Text S3).

The IRF (Text S4) was calculated at the bottom (BOA, surface) and top (TOA) of the atmosphere. The IRF differs by definition from the adjusted RF (readjustment of stratospheric temperatures) and the effective radiative forcing (ERF, allows for rapid adjustments within the climate system) (see, e.g., Myhre et al., 2013). For aerosols the IRF and RF values are similar (Hansen et al., 2007). The ERF is calculated using efficacies. For most constituents the efficacies are close to unity (Hansen et al., 2005), but it is large (2.1 – 4.5) for BC in snow (Flanner et al., 2007). We are not aware of efficacy values for dust in snow. Note that the IRF presented here represents the effect of all mineral dust rather than the anthropogenic contributions as often reported by the Intergovernmental Panel on Climate Change.

Longwave and shortwave irradiances were calculated using the uvspec model from the libRadtran software package (Emde et al., 2016; Mayer & Kylling, 2005). The independent column approximation was adopted and the radiative transfer equation solved using an improved version of DISORT (Buras et al., 2011; Stamnes et al., 1988) in pseudo-spherical geometry (Dahlback & Stamnes, 1991) with absorption by gases that was taken from the Fu and Liou (1992) parameterization.

To resolve the diurnal variations in solar zenith angle and temperature, IRF was calculated for every third hour. Area-averaged IRF calculated with 3-hr resolution differed by less than 0.5% from simulations with a 1-hr time resolution, though for individual pixels the differences were larger. Compared to typical IRF calculations in climate models, the adopted approach allows a more accurate treatment of the scattering phase function due to the use of more streams, and inclusion of scattering in the thermal part of the spectrum. Calculations of monthly IRF were made for the 10 dust source regions defined in Groot Zwaaftink et al. (2016) in addition to the sum of dust from all source regions, for latitudes north of 60°N on a 1° by 1° grid, see also Text S5.

3. Results and Discussions

The mineral dust BOA and TOA IRF for 2012 conditions are shown in Figure 1 (red lines). Both BOA and TOA IRF are bell-shaped and peak in April and May with IRF values of 0.479 and 0.787 W/m^2, respectively. From July onward the BOA IRF is close to zero. The TOA IRF is dominated by solar radiation from February to September, while between October and January both solar and thermal IRF are small (0.016 W/m^2). In the months of October to March, the thermal radiation gives a positive BOA IRF between 0.02 and 0.10 W/m^2 due to trapping of radiation by atmospheric dust. For the other months the BOA IRF is dominated by solar radiation. Negative BOA IRF without deposited dust is due to solar radiation being backscattered by the atmospheric dust. Several factors influence the annual variation of the TOA and BOA IRF, including the land area covered with snow, snow-covered sea ice area, deposited dust and atmospheric dust load (see Figure 2), and the solar ele-

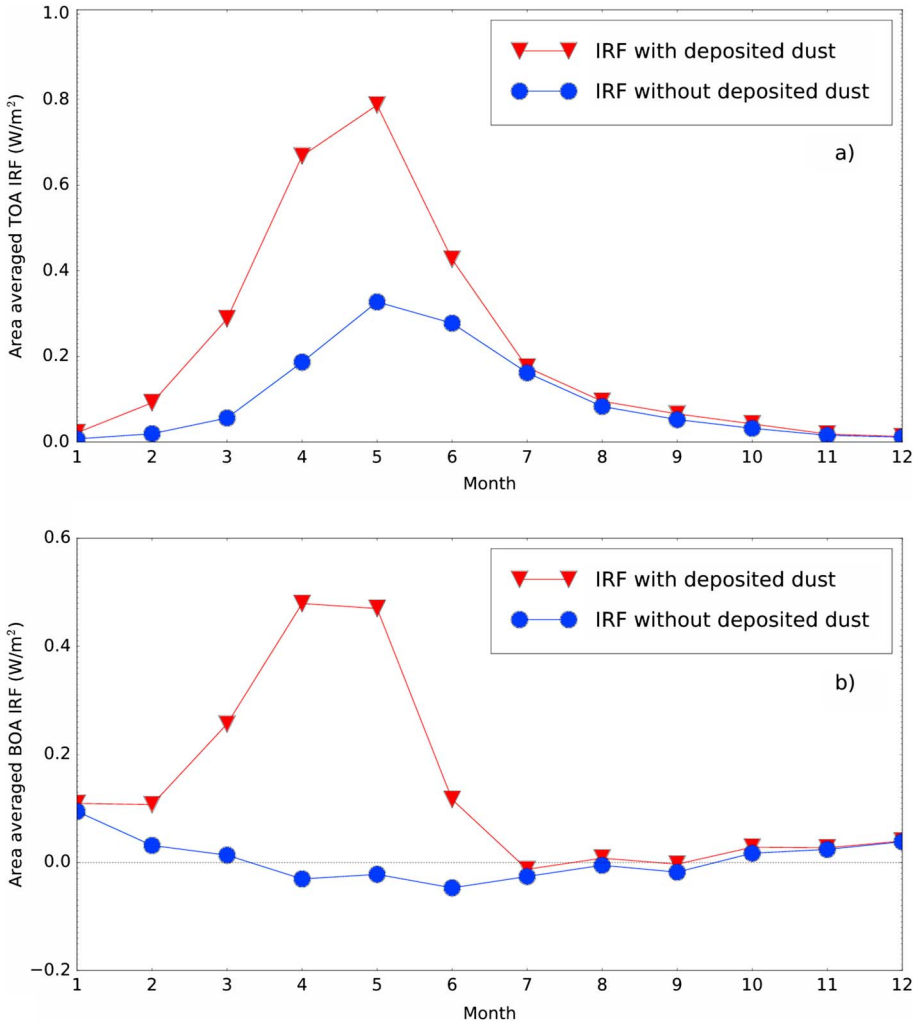

Figure 1. The area averaged (north of 60°N) dust (a) top of the atmosphere (TOA) and (b) bottom of the atmosphere (BOA) instantaneous radiative forcing (IRF) for 2012 conditions. The red (blue) curves show the IRF including (excluding) dust deposited on the surface. The black dotted line in panel (b) indicates the zero line.

vation. The IRF does not peak in June–July when the Sun is highest on the sky. Rather, the dust IRF is largest in April–May when both the atmospheric dust load and the amount of dust deposited on snow-covered surfaces, peak. Also, larger areas are covered with snow in April–May and earlier compared to June–July, which increases the albedo impact due to deposited dust. During winter, early spring, and late fall, the lack of sunlight weakens dust IRF. This is consistent with results of Goldenson et al. (2012) showing peak Arctic RF due to dust and BC deposition in snow and sea ice in May. The total annual dust TOA and BOA IRF are 0.225 and 0.135 W/m^2, respectively (see Table 1). The TOA IRF value is similar to corresponding values for BC as recently reviewed in Quinn et al. (2015).

The contributions to the Arctic TOA and BOA IRF from the individual dust sources are shown in Figure 3 and in Table 1. They are strongly linked to dust emission, transport and load, and deposition patterns for each source, as discussed by Groot Zwaaftink et al. (2016). The main contributors to the Arctic TOA IRF are dust from Asian sources south of 60°N (Asia S60) with ~29% and African sources (Africa) with ~19% (Figure 3a and Table 1). These regions are also globally by far the largest emission sources of dust (Figure S8c). The high-latitude sources contribute about 39% to the TOA IRF. The annual variation of TOA IRF due to distant dust sources (Africa; Asia S60) differs from that of the high-latitude sources North America north of 60°N (North America N60) and Europe and Asia north of 60°N (Eurasia N60), with the latter dropping relatively more in magnitude than the former after the month of June. Dust from high-latitude sources resides typically at lower altitudes than dust from distant sources (Groot Zwaaftink et al., 2016). Hence, dust from high-latitude sources

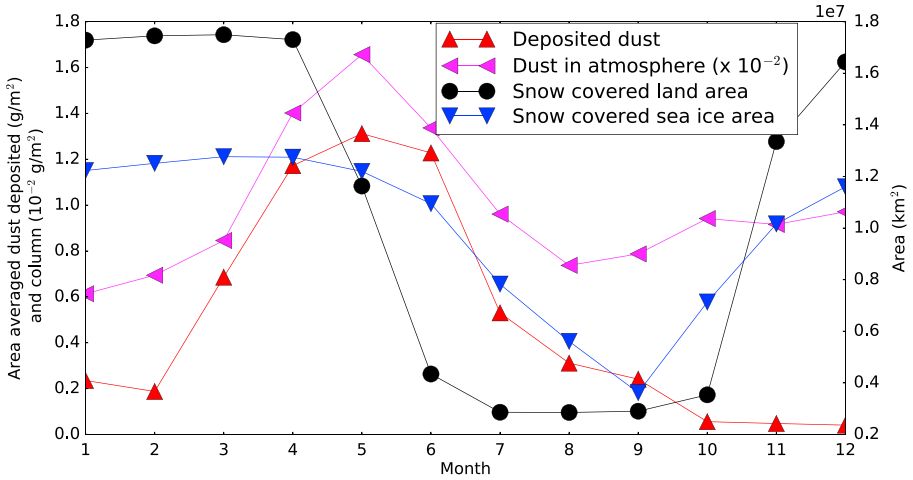

Figure 2. Annual variation of the land area covered by snow, the sea ice area covered by snow, the area-averaged monthly deposited dust (on snow covered areas), and the atmospheric dust column in the year 2012.

is readily deposited and its radiative impact is largest when there is snow on the ground. The area covered by snow drops rapidly between April and June and reaches its minimum in July when nearly only Greenland is snow covered (see Figure 2). This explains the rapid drop of TOA IRF due to dust from high-latitude sources from spring to summer. Dust from distant sources is more likely to stay aloft and thus causes smaller changes in albedo, which again implies that IRF due to dust aloft does not have an equally rapid drop when snow cover diminishes.

The BOA IRF (Figure 3b) is dominated by dust emitted from North America north of 60°N, Europe and Asia north of 60°N, Asia south of 60°N, and Africa. In total, the high-latitude sources contribute about 52% to the BOA IRF. The large dust sources in Africa and Asia south of 60°N contribute less than half, about 24%, of the

Table 1
Annual Dust BOA and TOA IRF (North of 60° N) for Various Dust Source Regions

Source region[a]	TOA (W/m^2)	BOA (W/m^2)	TOA efficiency (W/m^2)/(kg/month) 10^{-10}	BOA efficiency (W/m^2)/(kg/month) 10^{-10}
All	0.225	0.135		
All, snow covered land[b]		0.292		
All, snow covered sea ice[c]		0.020		
Africa	0.061	0.036	0.008	0.005
Asia S60	0.085	0.043	0.016	0.010
Australia	0.003	0.018	0.034	0.145
Europe S60	0.004	0.019	0.220	0.822
North America S60	0.008	0.020	0.041	0.090
South America	0.003	0.018	0.013	0.059
High-latitude dust sources				
Eurasia N60	0.046	0.060	0.751	0.877
Greenland	0.004	0.020	3.122	5.981
Iceland	0.005	0.020	0.831	1.306
North America N60	0.052	0.067	1.532	1.863

Note. The sum of IRF values from individual source regions is not equal to the IRF for "All" source regions, as IRF values cannot be simply added, due to nonlinearities. Percentage contributions from source regions to the total IRF reported in the text are calculated using the sum of the individual IRFs.
[a]Source regions as defined in Groot Zwaaftink et al. (2016). [b]Only snow covered land included in IRF. [c]Only snow covered sea ice included in IRF.

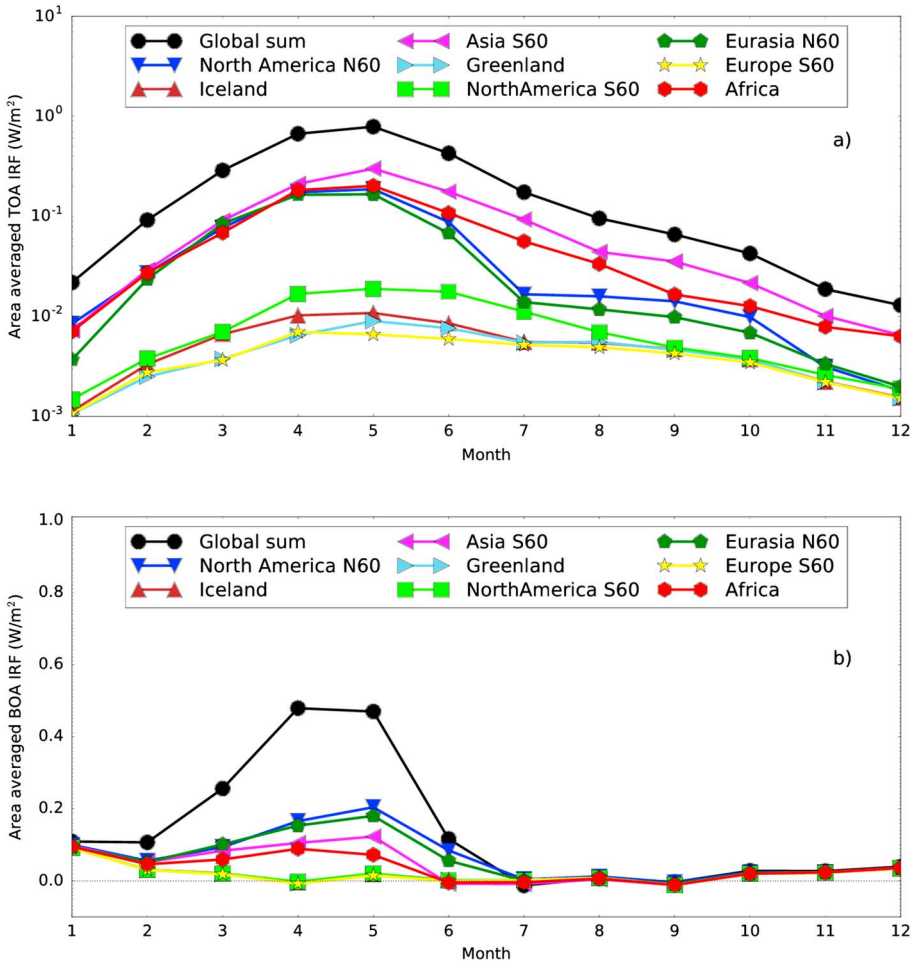

Figure 3. Individual contributions from various regions to the top of the atmosphere (TOA) (a) and bottom of the atmosphere (BOA) (b) dust instantaneous radiative forcing (IRF) for the year 2012. Note the logarithmic scale on *y* axis in panel (a). The black dotted line in panel (b) indicates the zero line.

high-latitude sources to the BOA IRF. This is due to the fact that high-latitude dust sources dominate the dust deposition in the Arctic and thus the snow albedo reduction.

The efficiency of a dust source region to affect the Arctic radiative environment may be estimated by dividing dust IRF by the amount of dust mass emitted in the region, Figures S8a and S8b and Table 1. The high-latitude sources (Eurasia N60, Greenland, Iceland, and North America N60) are 1 to 2 orders of magnitude more efficient in producing IRF in the Arctic. This should come as no surprise, as these dust sources are either within the Arctic or the dust from these sources needs to travel shorter distances and is thus more likely to reach the Arctic.

To assess the impact of deposited dust on IRF, TOA and BOA IRF simulations were made with and without dust deposited on the surface. Both cases included dust in the atmosphere. The monthly- and area-averaged TOA and BOA IRF values excluding deposited dust are shown in Figure 1 (blue lines). The contribution of the deposited dust to the TOA IRF is about 78%–80% for February and March; it is about 59% in May, when total IRF is largest; and less than 9% for July and August. The total annual dust TOA IRF is reduced from 0.225 to 0.103 W/m^2 when deposited dust is excluded. The BOA IRF is nearly entirely due to mineral dust deposited on the surface. The total annual dust BOA IRF is 0.135 W/m^2 (0.006 W/m^2) with (without) deposited dust. Lawrence et al. (2012) report global annual-mean IRF due to particles in the land-based snow pack of 0.037 W/m^2 for BC, 0.036 W/m^2 for mineral dust, and 0.083 W/m^2 for the combined effect of the two. For the months of March–May the combined effect is 1.5 W/m^2 over snow-covered regions. We only consider mineral dust north of 60°N in Figure 1, but note that our March–May average is 0.467 W/m^2 over snow-covered regions.

There is no unique definition of the Arctic. Above we have included all areas north of 60°N in the Arctic. Choosing a different definition of the Arctic, say the region north of 70°N, increases area-averaged TOA and BOA IRF values by about 6% and 10%, respectively. For further details, see Text S6.

From the evaluation of FLEXPART simulations, we assume that the model tends to overestimate dust deposition values at high altitudes in Greenland. This can lead to an overestimate of IRF in this region, although BOA IRF is relatively small here nonetheless (also see Text S5). Uncertainties of modeled dust deposition in other regions will also affect IRF estimates, but deposition observations at lower altitudes are necessary to assess this further. Hegg et al. (2009, 2010) identified BC from biomass sources as the main contributor to aerosol light absorption in snow. On the contrary, the modeled dust deposition results from Groot Zwaaftink et al. (2016) suggest that dust should be present in the Arctic. We note this discrepancy and urge further measurements of aerosol composition in Arctic snow.

To estimate the IRF uncertainty is difficult due to the many variables entering into the calculation and the lack of knowledge about the uncertainty of many of them. A simplified uncertainty estimate including dust load and deposition, snow grain size, snow depth, and dust optical properties, gives an IRF uncertainty of ±67% (Text S7). This is in line with Albani et al. (2014), which gives an overall uncertainty of 63% in TOA RF.

In this paper, we have used Arctic IRF as a measure of the potential impact of dust on Arctic climate. It is, however, not straightforward to convert Arctic IRF values into Arctic temperature responses. For instance, Flanner (2013) found that for BC the vertical distribution is extremely important. While a BC layer in the Arctic lower troposphere leads to Arctic surface warming, a BC layer in the upper troposphere cools the surface, even though both produce positive TOA IRF values. This means that high-latitude sources are more likely to produce Arctic surface warming, while low-latitude sources tend to cool the Arctic surface (see Figure 4.3 in Quinn et al., 2015). In addition, forcing outside the Arctic can change the heat transport into the Arctic and thus generate an Arctic temperature response (Sand et al., 2016). Nevertheless, the Arctic temperature response per unit of BC emission is largest for high-latitude source regions, which is due to larger Arctic IRF efficiency and, specifically, due to the more efficient deposition on Arctic snow, for BC from high-latitude sources (Sand et al., 2016). Our findings for BOA IRF efficiency for mineral dust are quite similar, indicating that high-latitude dust emissions lead to highly effective regional Arctic climate forcing, particularly via inducing snow albedo changes. The BOA IRF over snow-covered land surfaces is 0.292 W/m^2, Table 1, which may be compared to the estimates of BC 0.55–0.60 W/m^2 of Flanner et al. (2007, their central scenario, Table 3). The efficacy of mineral dust is presumably lower than for BC due to the lower single scattering albedo. Nevertheless, the estimated IRF due to mineral dust indicates that mineral dust may be important in the Arctic climate.

It is important to notice that high-latitude dust sources generally are neglected or seem not to be very active in global climate models (Albani et al., 2014; Mahowald et al., 2006; Zender et al., 2003), despite recordings of highly active dust sources in, for instance, Iceland (e.g., Arnalds et al., 2016). These models may thus substantially underestimate BOA RF due to dust in the Arctic. In addition, many climate models do not account for snow albedo changes. Both these shortcomings will cause the models to underestimate the climate impacts of dust in the Arctic. It would thus be urgent to quantify the climate impact of changing dust sources at high latitudes, including their effect on snow albedo.

4. Conclusions

Using recent dust load estimates from Groot Zwaaftink et al. (2016), bottom and top of the atmosphere mineral dust radiative forcing values have been calculated for latitudes north of 60°N for 2012. We find the annual direct mineral dust IRF in the Arctic to be 0.225 and 0.135 W/m^2 at the TOA and BOA, respectively. For snow-covered land surfaces the BOA IRF is 0.292 W/m^2, about half of the BC central scenario estimate of Flanner et al. (2007). The largest individual source contributions to the TOA mineral dust IRF come from dust transported from Asia south of 60°N (∼29%) and Africa (∼19%), while all high-latitude dust sources contribute ∼39% to the TOA IRF. The albedo reduction due to deposited mineral dust accounts for more than half of the TOA IRF when there is snow on the ground. In terms of Arctic IRF efficiency, that is, TOA IRF in the Arctic per emitted kilogram of mineral dust, high-latitude (>60°N) dust sources are about 1 to 2 orders of magnitude more efficient than lower-latitude dust sources.

Mineral dust deposited on snow accounts for nearly all (∼99%) of the BOA IRF. The high-latitude dust sources contribute ∼52% of the annual Arctic BOA IRF and ∼39% to the TOA IRF. This difference is explained by the

fact that dust from high-latitude sources resides mainly in the lower troposphere and is effectively deposited at the surface. The high-latitude dust sources in North America, Europe and Asia north of 60°N are the largest contributors to the BOA IRF. Dust sources in Greenland have the largest BOA and TOA forcing efficiencies.

From the evaluation of FLEXPART simulations, the model possibly tends to overestimate dust deposition values at high altitudes in Greenland. This can lead to an overestimate of IRF in this region, although BOA IRF there is relatively small nonetheless. Rather, our calculations probably underestimate true IRF of mineral dust in the Arctic. First, we have assumed the same optical properties for all mineral dust sources. However, for example Icelandic dust originates from basaltic material and is darker than dust from the main desert regions (e.g., Arnalds et al., 2016). Thus, it may have a larger impact on IRF than calculated here. This may to some extent also be true for other high-latitude dust source regions. Second, for the year studied, 2012, the Arctic sea ice extent was at its minimum. In other years with more sea ice, dust IRF may be larger. However, our assumption that all sea ice is snow covered, may overestimate IRF.

By extrapolating climate response calculations published for low-altitude BC, the effective BOA IRF caused by high-latitude dust sources indicates that they may produce a substantial surface warming and effectively trigger Arctic feedback processes partly responsible for Arctic amplification. Since climate models generally seem to underestimate high-latitude dust sources and many such models do not simulate snow albedo effects, they may substantially underestimate BOA IRF and climate impacts of mineral dust in the Arctic.

Acknowledgments
M. G. Flanner is kindly acknowledged for making the SNICAR model available (http://snow.engin.umich.edu/). Mineral dust data are from Groot Zwaaftink et al. (2016) and available upon request. The FLEXPART source code is available from www.flexpart.eu. The libRadtran model is available from www.libradtran.org. A. K. acknowledges support from the Research Council of Norway (contract 262637). C. D. G. Z. acknowledges funding provided by the Swiss National Science Foundation. C. D. G. Z. and A. S. were partly supported by Nordforsk in the Nordic Center of Excellence eSTICC (Nordforsk 57001). Thanks to the two anonymous reviewers whose valuable comments greatly improved the paper.

References

Albani, S., Mahowald, N. M., Perry, A. T., Scanza, R. A., Zender, C. S., Heavens, N. G., et al. (2014). Improved dust representation in the Community Atmosphere Model. *Journal of Advances in Modeling Earth Systems*, *6*, 541–570.

Aoki, T., Hori, M., Motoyoshi, H., Tanikawa, T., Hachikubo, A., Sugiura, K., et al. (2007). ADEOS-II/GLI snow/ice products—Part II: Validation results using GLI and MODIS data. *Remote Sensing of Environment*, *111*(2-3), 274–290. https://doi.org/10.1016/j.rse.2007.02.035

Arnalds, O., Dagsson-Waldhauserova, P., & Olafsson, H. (2016). The Icelandic volcanic aeolian environment: Processes and impacts—A review. *Aeolian Research*, *20*, 176–195. https://doi.org/10.1016/j.aeolia.2016.01.004

Balkanski, Y., Schulz, M., Claquin, T., & Guibert, S. (2007). Reevaluation of mineral aerosol radiative forcings suggests a better agreement with satellite and aeronet data. *Atmospheric Chemistry and Physics*, *7*(1), 81–95. https://doi.org/10.5194/acp-7-81-2007

Bindoff, N., Stott, P., AchutaRao, K., Allen, M., Gillett, N., Gutzler, D., et al. (2013). Detection and attribution of climate change: From global to regional. In T. F. Stocker, et al. (Eds.), *Climate change 2013: The physical science basis. Contribution of Working Group I to the Fifth Assessment Report of the Intergovernmental Panel on Climate Change*. Cambridge, UK and New York: Cambridge University Press.

Bullard, J. E., Baddock, M., Bradwell, T., Crusius, J., Darlington, E., Gaiero, D., et al. (2016). High-latitude dust in the Earth system. *Reviews of Geophysics*, *54*, 447–485. https://doi.org/10.1002/2016RG000518

Buras, R., Dowling, T., & Emde, C. (2011). New secondary-scattering correction in DISORT with increased efficiency for forward scattering. *Journal of Quantitative Spectroscopy and Radiative Transfer*, *112*, 2028–2034. https://doi.org/10.1016/j.jqsrt.2011.03.019

Dahlback, A., & Stamnes, K. (1991). A new spherical model for computing the radiation field available for photolysis and heating at twilight. *Planetary and Space Science*, *39*, 671–683.

Dumont, M., Brun, E., Picard, G., Michou, M., Libois, Q., Petit, J.-R., et al. (2014). Contribution of light-absorbing impurities in snow to Greenland's darkening since 2009. *Nature Geoscience*, *7*(7), 509–512.

Emde, C., Buras-Schnell, R., Kylling, A., Mayer, B., Gasteiger, J., Hamann, U., et al. (2016). The libRadtran software package for radiative transfer calculations (version 2.0.1). *Geoscientific Model Development*, *9*(5), 1647–1672. https://doi.org/10.5194/gmd-9-1647-2016

Flanner, M. G. (2013). Arctic climate sensitivity to local black carbon. *Journal of Geophysical Research: Atmospheres*, *118*, 1840–1851. https://doi.org/10.1002/jgrd.50176

Flanner, M. G., Zender, C. S., Hess, P. G., Mahowald, N. M., Painter, T. H., Ramanathan, V., & Rasch, P. J. (2009). Springtime warming and reduced snow cover from carbonaceous particles. *Atmospheric Chemistry and Physics*, *9*(7), 2481–2497. https://doi.org/10.5194/acp-9-2481-2009

Flanner, M. G., Zender, C. S., Randerson, J. T., & Rasch, P. J. (2007). Present-day climate forcing and response from black carbon in snow. *Journal of Geophysical Research*, *112*, D11202. https://doi.org/10.1029/2006JD008003

Fu, Q., & Liou, K. N. (1992). On the correlated *k*-distribution method for radiative transfer in nonhomogeneous atmospheres. *Journal of the Atmospheric Sciences*, *49*, 2139–2156.

Goldenson, N., Doherty, S. J., Bitz, C. M., Holland, M. M., Light, B., & Conley, A. J. (2012). Arctic climate response to forcing from light-absorbing particles in snow and sea ice in CESM. *Atmospheric Chemistry and Physics*, *12*(17), 7903–7920. https://doi.org/10.5194/acp-12-7903-2012

Groot Zwaaftink, C. D., Arnalds, O., Dagsson-Waldhauserova, P., Eckhardt, S., Prospero, J. M., & Stohl, A. (2017). Temporal and spatial variability of Icelandic dust emissions and atmospheric transport. *Atmospheric Chemistry and Physics*, *17*, 10,865–10,878. https://doi.org/10.5194/acp-17-10865-2017

Groot Zwaaftink, C. D., Grythe, H., Skov, H., & Stohl, A. (2016). Substantial contribution of northern high-latitude sources to mineral dust in the Arctic. *Journal of Geophysical Research: Atmospheres*, *121*(22), 13,678–13,697. https://doi.org/10.1002/2016JD025482

Grythe, H., Kristiansen, N. I., Groot Zwaaftink, C. D., Eckhardt, S., Stroem, J., Tunved, P., et al. (2017). A new aerosol wet removal scheme for the Lagrangian particle model FLEXPART v10. *Geoscientific Model Development*, *10*, 1447–1466. https://doi.org/10.5194/gmd-10-1447-2017

Hansen, J., Sato, M., Ruedy, R., Kharecha, P., Lacis, A., Miller, R., et al. (2007). Climate simulations for 1880–2003 with GISS modelE. *Climate Dynamics*, *29*(7), 661–696. https://doi.org/10.1007/s00382-007-0255-8

Hansen, J., Sato, M., Ruedy, R., Nazarenko, L., Lacis, A., Schmidt, G. A., et al. (2005). Efficacy of climate forcings. *Journal of Geophysical Research*, *110*, D18104. https://doi.org/10.1029/2005JD005776

Hegg, D. A., Warren, S. G., Grenfell, T. C., Doherty, S. J., & Clarke, A. D. (2010). Sources of light-absorbing aerosol in arctic snow and their seasonal variation. *Atmospheric Chemistry and Physics*, *10*(22), 10,923–10,938. https://doi.org/10.5194/acp-10-10923-2010

Hegg, D. A., Warren, S. G., Grenfell, T. C., Doherty, S. J., Larson, T. V., & Clarke, A. D. (2009). Source attribution of black carbon in arctic snow. *Environmental Science and Technology*, *43*(11), 4016–4021. https://doi.org/10.1021/es803623f

Hess, M., Koepke, P., & Schult, I. (1998). Optical properties of aerosols and clouds: The software package OPAC. *Bulletin of the American Meteorological Society*, *79*, 831–844.

Hori, M., Aoki, T., Stamnes, K., & Li, W. (2007). ADEOS-II/GLI snow/ice products—Part III: Retrieved results. *Remote Sensing of Environment*, *111*(2-3), 291–336. https://doi.org/10.1016/j.rse.2007.01.025

Kern, S., Khvorostovsky, K., Skourup, H., Rinne, E., Parsakhoo, Z. S., Djepa, V., et al. (2015). The impact of snow depth, snow density and ice density on sea ice thickness retrieval from satellite radar altimetry: Results from the ESA-CCI Sea Ice ECV project round robin exercise. *The Cryosphere*, *9*(1), 37–52. https://doi.org/10.5194/tc-9-37-2015

Key, J. R., Yang, P., Baum, B. A., & Nasiri, S. L. (2002). Parameterization of shortwave ice cloud optical properties for various particle habits. *Journal of Geophysical Research*, *107*(D13), 4181. https://doi.org/10.1029/2001JD000742

Kok, J. F. (2011). A scaling theory for the size distribution of emitted dust aerosols suggests climate models underestimate the size of the global dust cycle. *Proceedings of the National Academy of Sciences of the United States of America*, *108*(3), 1016–1021. https://doi.org/10.1073/pnas.1014798108

Lambert, F., Kug, J.-S., Park, R. J., Mahowald, N., Winckler, G., Abe-Ouchi, A., et al. (2013). The role of mineral-dust aerosols in polar temperature amplification. *Nature Climate Change*, *3*(5), 487–491. https://doi.org/10.1038/nclimate1785

Lawrence, D. M., Oleson, K. W., Flanner, M. G., Fletcher, C. G., Lawrence, P. J., Levis, S., et al. (2012). The CCSM4 land simulation, 1850–2005: Assessment of surface climate and new capabilities. *Journal of Climate*, *25*, 2240–2260.

Mahowald, N. M., Muhs, D. R., Levis, S., Rasch, P. J., Yoshioka, M., Zender, C. S., & Luo, C. (2006). Change in atmospheric mineral aerosols in response to climate: Last glacial period, preindustrial, modern, and doubled carbon dioxide climates. *Journal of Geophysical Research*, *111*, D10202. https://doi.org/10.1029/2005JD006653

Marticorena, B., & Bergametti, G. (1995). Modeling the atmospheric dust cycle: 1. Design of a soil-derived dust emission scheme. *Journal of Geophysical Research*, *100*(D8), 16,415–16,430. https://doi.org/10.1029/95JD00690

Martin, G. M., Johnson, D. W., & Spice, A. (1994). The measurement and parameterization of effective radius of droplets in warm stratocumulus clouds. *Journal of the Atmospheric Sciences*, *51*, 1823–1842.

Mayer, B., & Kylling, A. (2005). Technical note: The libRadtran software package for radiative transfer calculations—Description and examples of use. *Atmospheric Chemistry and Physics*, *5*, 1855–1877.

McFarquhar, G. M., Iacobellis, S., & Somerville, R. C. J. (2003). SCM simulations of tropical ice clouds using observationally based parameterizations of microphysics. *Journal of Climate*, *16*, 1643–1664.

Myhre, G., Shindell, D., Bréon, F.-M., Collins, W., Fuglestvedt, J., Huang, J., et al. (2013). Anthropogenic and natural radiative forcing. In T. F. Stocker et al. (Eds.), *Climate change 2013: The physical science basis. Contribution of Working Group I to the Fifth Assessment Report of the Intergovernmental Panel on Climate Change*. Cambridge, UK and New York: Cambridge University Press.

Nousiainen, T. (2009). Optical modeling of mineral dust particles: A review. *Journal of Quantitative Spectroscopy and Radiative Transfer*, *110*(14-16), 1261–1279. https://doi.org/10.1016/j.jqsrt.2009.03.002

Qian, Y., Yasunari, T. J., Doherty, S. J., Flanner, M. G., Lau, W. K. M., Ming, J., et al. (2015). Light-absorbing particles in snow and ice: Measurement and modeling of climatic and hydrological impact. *Advances in Atmospheric Sciences*, *32*, 64–91. https://doi.org/10.1007/s00376-014-0010-0

Quinn, P. K., Stohl, A., Arnold, S., Baklanov, A., Berntsen, T. K., Christensen, J. H., et al. (2015). AMAP assessment 2015: Black carbon and ozone as Arctic climate forcers. Arctic Monitoring and Assessment Programme (AMAP) (vii + 116pp.). Oslo, Norway.

Räisänen, P., Haapanala, P., Chung, C. E., Kahnert, M., Makkonen, R., Tonttila, J., & Nousiainen, T. (2013). Impact of dust particle non-sphericity on climate simulations. *Quarterly Journal of the Royal Meteorological Society*, *139*(677), 2222–2232. https://doi.org/10.1002/qj.2084

Sand, M., Berntsen, T. K., von Salzen, K., Flanner, M. G., Langner, J., & Victor, D. G. (2016). Arctic climate sensitivity to local black carbon. *Nature Climate Change*, *6*, 286–289.

Serreze, M. C., & Francis, J. A. (2006). The arctic amplification debate. *Climatic Change*, *76*(3), 241–264. https://doi.org/10.1007/s10584-005-9017-y

Shao, Y., & H. Lu (2000). A simple expression for wind erosion threshold friction velocity. *Journal of Geophysical Research*, *105*(D17), 22,437–22,443. https://doi.org/10.1029/2000JD900304

Stamnes, K., Li, W., Eide, H., Aoki, T., Hori, M., & Storvold, R. (2007). ADEOS-II/GLI snow/ice products—Part i: Scientific basis. *Remote Sensing of Environment*, *111*(2–3), 258–273. https://doi.org/10.1016/j.rse. 2007.03.023

Stamnes, K., Tsay, S.-C., Wiscombe, W., & Jayaweera, K. (1988). Numerically stable algorithm for discrete–ordinate–method radiative transfer in multiple scattering and emitting layered media. *Applied Optics*, *27*, 2502–2509.

Stohl, A., Forster, C., Frank, A., Seibert, P., & Wotawa, G. (2005). Technical note: The Lagrangian particle dispersion model FLEXPART version 6.2. *Atmospheric Chemistry and Physics*, *5*, 2461–2474.

Varotsos, C. A., Melnikova, I. N., Cracknell, A. P., Tzanis, C., & Vasilyev, A. V. (2014). New spectral functions of the near-ground albedo derived from aircraft diffraction spectrometer observations. *Atmospheric Chemistry and Physics*, *14*(13), 6953–6965. https://doi.org/10.5194/acp-14-6953-2014

Wang, Z., Zhang, H., Jing, X., & Wei, X. (2013). Effect of non-spherical dust aerosol on its direct radiative forcing. *Atmospheric Research*, *120-121*, 112–126. https://doi.org/10.1016/j.atmosres.2012.08.006

Wiscombe, W. J., & Warren, S. G. (1980). A model for the spectral albedo of snow, I, Pure snow. *Journal of the Atmospheric Sciences*, *37*, 2712–2733.

Wittmann, M., Groot Zwaaftink, C. D., Schmidt, L. S., S. Guðmundsson, F. Pálsson, O. Arnalds, et al. (2017). Impact of dust deposition on the albedo of Vatnajökull ice cap, Iceland. *The Cryosphere*, *11*(2), 741–754.

Wyser, K. (1998). The effective radius in ice clouds. *Journal of Climate*, *11*, 1793–1802.

Yang, P., Wei, H., Huang, H.-L., Baum, B., Hu, Y. X., Kattawar, G. W., et al. (2005). Scattering and absorption property database for nonspherical ice particles in the near- through far-infrared spectral region. *Applied Optics*, *44*, 5512–5523.

Yi, B., Hsu, C. N., Yang, P., & Tsay, S.-C. (2011). Radiative transfer simulation of dust-like aerosols: Uncertainties from particle shape and refractive index. *Journal of Aerosol Science*, *42*(10), 631–644. https://doi.org/10.1016/j.jaerosci.2011.06.008

Zender, C. S., Bian, H., & Newman, D. (2003). Mineral dust entrainment and deposition (DEAD) model: Description and 1990s dust climatology. *Journal of Geophysical Research*, *108*(D14), 4416. https://doi.org/10.1029/2002JD002775